
IASI NRT HNO₃ VALIDATION REPORT

Validated products:

Identifier	Name	Acronym
O3M-81	IASI B Near Real Time HNO ₃	MBI-N-HNO3
O3M-336	IASI C Near Real Time HNO ₃	MCI-N-HNO3

Authors:

Name
Bavo Langerock

Institute
Belgian Institute for Space Aeronomy

Reporting period: December 2019 – December 2021

Input data versions: IASI/Metop NRT EumetCAST BUFR_IASI_NAC

Data processor versions: FORLI-HNO3 v20151001_2

authors B. Langerock

reference SAF/AC/IASB/VR/HNO3/ValidationReport_HNO3_ORR_MetopB/C

document type AC-SAF Validation Report

issue 1

revision 1

date of issue 26 April 2022

products MBI-N-HNO3, MCI-N-HNO3

product version FORLI-HNO3 v20151001_2

distribution

Function	Organisation
AC-SAF	EUMETSAT, BIRA-IASB, DLR, DMI, DWD, FMI, HNMS/AUTH, KNMI, RMI

external contributors

NDACC teams contributing ground-based correlative measurements

Acronym	Organisation	Country
BIRA.IASB	Belgian Institute for Space Aeronomy	BELGIUM
IUP	Institut fuer Umwelphysik, Universitaet Bremen	GERMANY
KIT	Karlsruhe Institute of Technology	GERMANY
KIT.IMK.IFU	Karlsruhe Institute of Technology - Institute for Meteorology and Climate Research - Atmospheric Environmental Research	GERMANY
NCAR	National Center for Atmospheric Research	UNITED STATES
NIWA	National Institute of Water and Atmospheric Research	NEW ZEALAND
SPBU	Saint Petersburg State University	RUSSIAN FEDERATION
ULG	University of Liege	BELGIUM
UNAGOYA	University of Nagoya	JAPAN
UNAM	Universidad Nacional Autonoma de Mexico	MEXICO
UOW	University of Wollongong	AUSTRALIA
UTORONTO	University of Toronto	CANADA

document change record

Issue	Rev.	Date	Section	Description of Change
1	0	22.12.2021	-	Creation of this document
1	1	26.04.2022	-	Inclusion of reviewer comments

AC SAF product ID numbers

AC SAF internal identifier	Description
IASI NRT HNO3	O3M-81, O3M-336

Validation report of IASI NRT HNO₃ for Metop-B and C Operational Readiness Review

CONTENTS

ACRONYMS AND ABBREVIATIONS	4
1. INTRODUCTION	6
1.1. Scope of this document	6
2. VALIDATION WITH NDACC GROUND-BASED FTIR HNO₃ DATA.....	7
2.1. Measurement characterisation	7
2.2. Comparison methodology	10
2.3. Comparison statistics.....	12
3. DISCUSSION AND CONCLUSIONS.....	15
4. REFERENCES	17
4.1. Applicable documents	17
4.2. Reference documents.....	17

ACRONYMS AND ABBREVIATIONS

AVK	Averaging kernel
AC SAF	Atmospheric Composition Monitoring Satellite Application Facility CDOP-3: Third Continuous Development and Operations Phase
CNRS/LATMOS	Laboratoire Atmosphère, Milieux, Observations Spatiales du CNRS
PC	Partial Column
ESA	European Space Agency
EUMETSAT	European Organisation for the Exploitation of Meteorological Satellites
BIRA-IASB	Institut d'Aéronomie Spatiale de Belgique
IASI	Infrared Atmospheric Sounding Interferometer
IFE/IUP	Institut für Fernerkundung/Institut für Umweltphysik
INTA	Instituto Nacional de Técnica Aeroespacial
FORLI	Fast Optimal Retrievals on Layers for IASI
LOS	Line Of Sight
NDACC	Network for the Detection of Atmospheric Composition Change
NIWA	National Institute for Water and Atmospheric research
O3M-SAF	Ozone and Atmospheric Chemistry Monitoring Satellite Application Facility
SNR	Signal to Noise Ratio
SZA	Solar Zenith Angle
TOA	Top Of the Atmosphere
ULB	Université Libre de Bruxelles
VCD	Vertical Column Density
VMR	Volume Mixing Ratio
WMO	World Meteorological Organization

Introduction to EUMETSAT Satellite Application Facility on Atmospheric Composition monitoring (AC SAF)

Background

The monitoring of atmospheric chemistry is essential due to several human caused changes in the atmosphere, like global warming, loss of stratospheric ozone, increasing UV radiation, and pollution. Furthermore, the monitoring is used to react to the threats caused by the natural hazards as well as follow the effects of the international protocols.

Therefore, monitoring the chemical composition and radiation of the atmosphere is a very important duty for EUMETSAT and the target is to provide information for policy makers, scientists and general public.

Objectives

The main objectives of the AC SAF is to process, archive, validate and disseminate atmospheric composition products (O₃, NO₂, SO₂, BrO, HCHO, H₂O, OCIO, CO, NH₃), aerosol products and surface ultraviolet radiation products utilising the satellites of EUMETSAT. The majority of the AC SAF products are based on data from the GOME-2 and IASI instruments onboard Metop satellites.

Another important task besides the near real-time (NRT) and offline data dissemination is the provision of long-term, high-quality atmospheric composition products resulting from reprocessing activities.

Product categories, timeliness and dissemination

NRT products are available in less than three hours after measurement. These products are disseminated via EUMETCast, WMO GTS or internet.

- Near real-time trace gas columns (total and tropospheric O₃ and NO₂, total SO₂, total HCHO, CO) and high-resolution ozone profiles
- Near real-time absorbing aerosol indexes from main science channels and polarization measurement detectors
- Near real-time UV indexes, clear-sky and cloud-corrected

Offline products are available within two weeks after measurement and disseminated via dedicated web services at EUMETSAT and AC SAF.

- Offline trace gas columns (total and tropospheric O₃ and NO₂, total SO₂, total BrO, total HCHO, total H₂O) and high-resolution ozone profiles
- Offline absorbing aerosol indexes from main science channels and polarization measurement detectors
- Offline surface UV, daily doses and daily maximum values with several weighting functions

Data records are available after reprocessing activities from the EUMETSAT Data Centre and/or the AC SAF archives.

- Data records generated in reprocessing
- Lambertian-equivalent reflectivity
- Total OCIO

Users can access the AC SAF offline products and data records (free of charge) by registering at the AC SAF web site.

More information about the AC SAF project, products and services: <https://acsaf.org/>

AC SAF Helpdesk: helpdesk@acsaf.org

Twitter: https://twitter.com/Atmospheric_SAF

1. INTRODUCTION

1.1. Scope of this document

The present document reports on the verification and validation of Metop-B and C NRT HNO₃ data over the Dec 2019 – Dec. 2021 time period, produced by the FORLI Data Processor version FORLI-HNO3 v20151001_2 operated at EUMETSAT. This report includes verification work performed using ground-based nitric acid profile measurements from the NDACC network. The aim is to investigate whether the IASI NRT HNO₃ data product fulfils the product requirements in terms of accuracy (Threshold accuracy: 50%; Target accuracy: 35%; Optimal: 10%), as stated in the FORLI-HNO3 product specification, requirement and assessment document [AD1] and in the Product Requirements Document [AD2].

2. VALIDATION WITH NDACC GROUND-BASED FTIR HNO₃ DATA

This chapter discusses in detail the comparison between the IASI NRT HNO₃ operational product against FTIR measurement data publicly available from the NDACC (Network for the Detection of Atmospheric Composition Change) data base. All available data since the release of the IASI HNO₃ product in the NRT data streams in Dec 2019 is used. Sixteen NDACC sites provide HNO₃ data during this period (Figure 2.1 and Figure 2.2).

The validation methodology largely follows the setup used in Ronsmans *et al.*, 2016. Sections 2.1 and 2.2 describe the main characteristics of the measurements used in the comparison and the comparison methodology. Deviations from the methodology in Ronsmans *et al.*, 2016 are explicitly mentioned.

2.1. Measurement characterisation

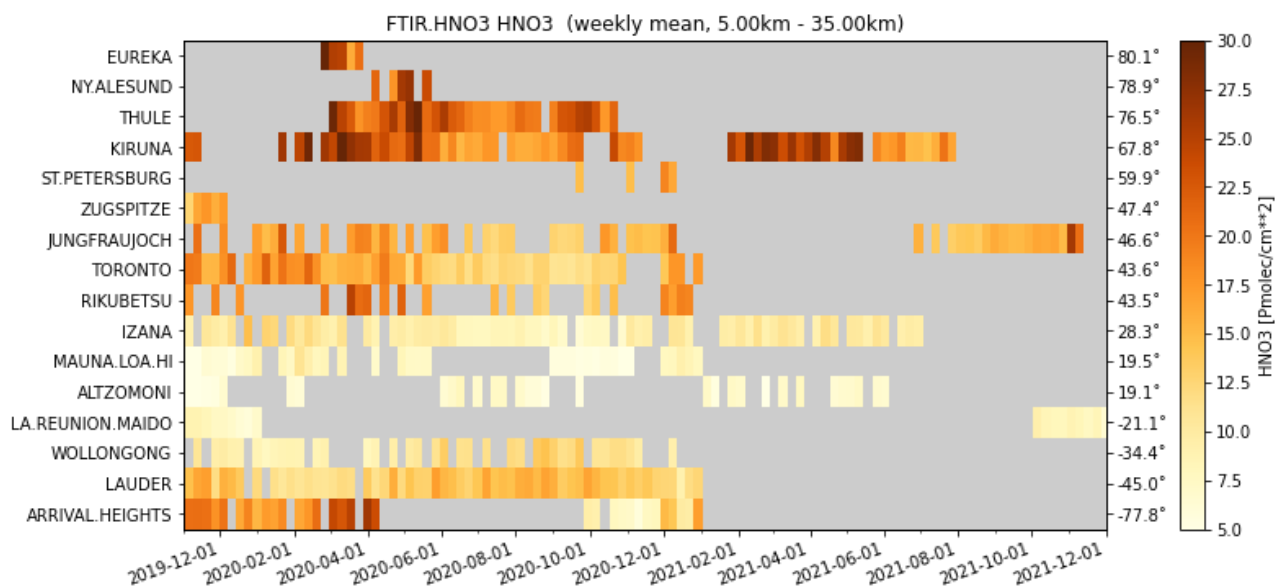


Figure 2.1 Overview of NDACC instruments with HNO₃ measurement data since end 2019. Time series shows partial columns of HNO₃ between 5km and 35km. Sites are sorted by latitude which is indicated on the right. FTIR measures direct sunlight and hence no measurements are available at high latitude stations during local winter.

NDACC FTIR

Although reported as profiles, NDACC FTIR HNO₃ measurements are sensitive to the stratosphere between approximately 10 and 35km. NDACC HNO₃ data is formatted in GEOMS hdf files which contain a.o. the retrieved HNO₃ VMR profiles between the surface and the top of the atmosphere (TOA), the associated averaging kernels and *a-priori* profiles. An example FTIR averaging kernel is shown in Figure 2.6 including the sensitivity curve. The *a-priori* profiles are obtained from the Whole Atmosphere Community Climate Model (WACCM) model.

The typical total column uncertainty on the FTIR HNO₃ data is approximately 8% and increases to 12% at high latitude sites. Figure 2.1 provides an overview of all NDACC HNO₃ data for the mentioned time period as partial columns HNO₃ between 5km and 35km. All FTIR spectrometers are Bruker type spectrometers, except the instrument at Toronto which is a Bomem spectrometer. For further details on the instruments, we

refer to Vigouroux *et al.*, 2020. Typical values for the FTIR degrees of freedom (DOF) are approximately 2 for latitudes between -50 and 50 degrees north and increase up to 3 for high latitude stations.

For further details on the NDACC FTIR data, see Vigouroux *et al.*, 2007.

IASI FORLI

Similar as NDACC FTIR profiles, IASI FORLI HNO₃ profiles are obtained by optimal estimation (Rodgers 2000) and the associated averaging kernels and *a-priori* profiles are distributed in the NRT BUFR files (see HNO₃ PUM). The quality filter proposed in the PUM is applied and only pixels with QFLAG>0 are taken into account. The IASI *a-priori* profile is derived from daily profiles from the LMDz-INCA chemistry transport model (from the ground up to 15.6 km) and of all profiles obtained from ACE-FTS (from 6 to 60 km) Hurtmans *et al.* (2012). As mentioned in Wespes *et al.* (2009) and Ronsmans *et al.* (2016), the limited sensitivity in the FORLI retrieval does not allow deducing multiple pieces of vertical information. Therefore all statistics in this report will be based on partial columns covering the IASI sensitivity range (5km -35km). The maximum sensitivity is reached at 15km and coincided with the UTLS for the tropical sites and the lower/mid stratosphere for the higher latitudes, see Figure 2.5 for typical pixel averaging kernels and Ronsmans *et al.* (2016).

The IASI DOFS reached at the NDACC sites is shown in Figure 2.4 and are close to 1 and are 0.9 at the high latitude sites and increase to 1.1 DOFS at the tropical sites. No NDACC site coincides with the (possibly questionable) higher DOFS ~ 1.2 mentioned in Ronsmans *et al.* (2016).

The total uncertainty is estimated in Ronsmans *et al.* (2016) at 8-10% and becomes larger at tropical site (10-15%) due to interference of higher water concentrations.

Figure 2.2 shows the IASI-B HNO₃ columns at the different NDACC sites. The difference between the IASI retrieved and *a priori* columns is shown in Figure 2.3. The overestimation of the IASI prior at the tropical sites is a systematic geographical pattern and is this is the key argument in the validation setup to deviate from the validation methodology used in Ronsmans *et al.*, 2016, as described in the next section.

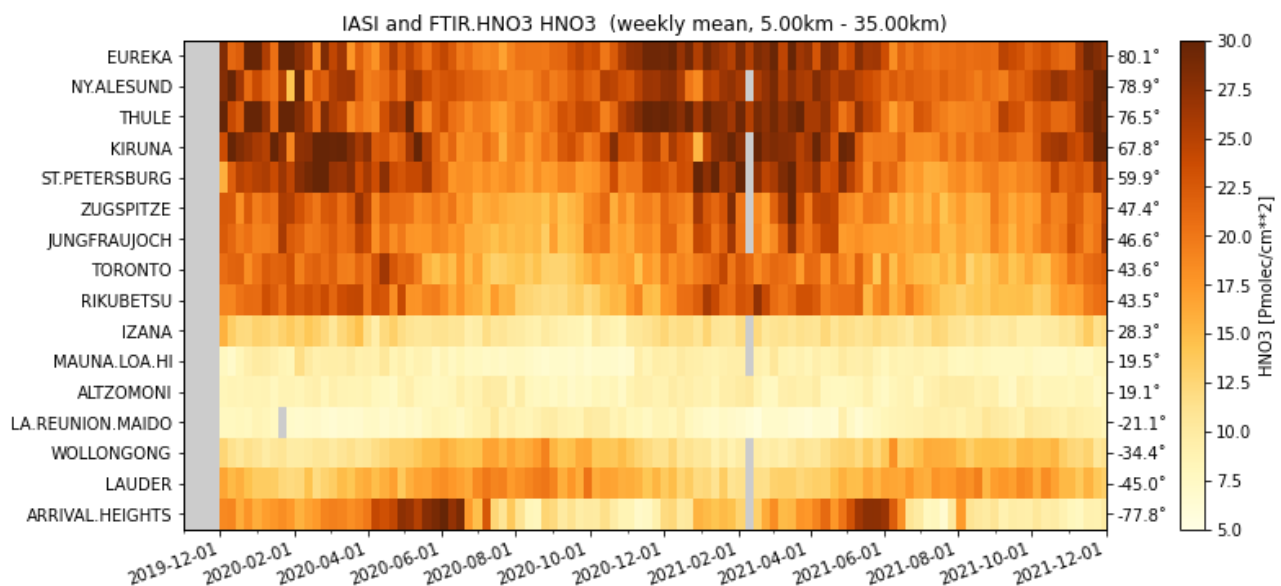


Figure 2.2 Mosaic of IASI-B HNO₃ partial columns between 5km and 35km at the different NDACC sites for the period 2020-2021. Similar to Figure 2.1, sites are sorted according to latitude.

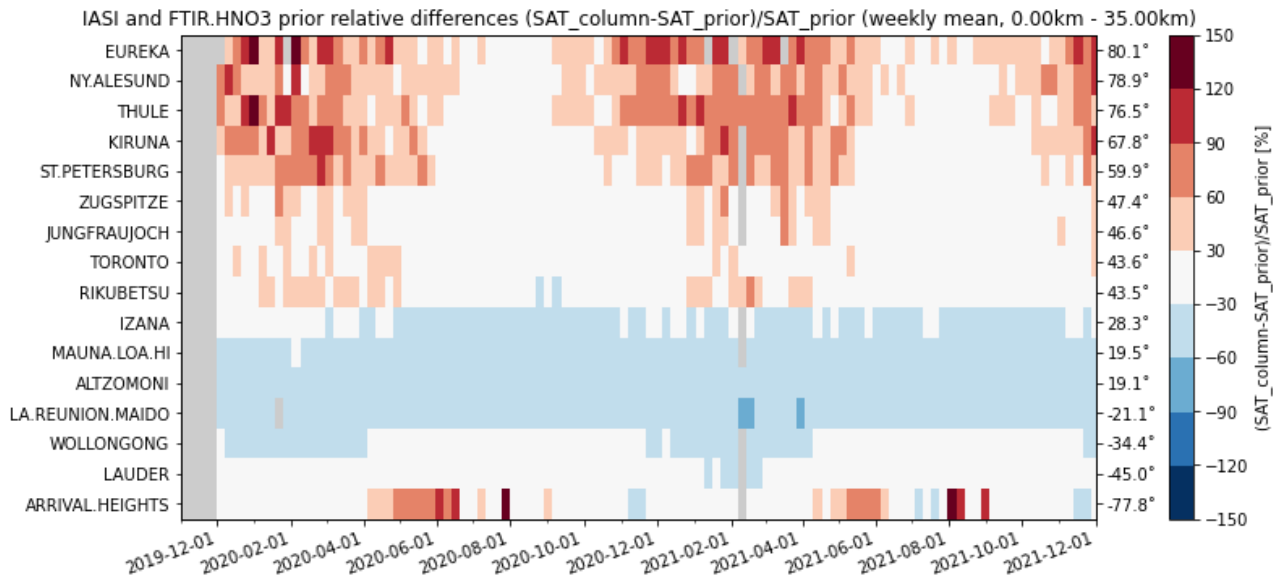


Figure 2.3 Mosaic of IASI-B HNO₃ relative differences between retrieved and *a priori* columns at the different NDACC sites for the period 2020-2021. Similar to Figure 2.1, sites are sorted according to latitude. The IASI prior is underestimating the retrieved columns at high latitude sites during local winter and overestimating in the tropical region with values above -40%.

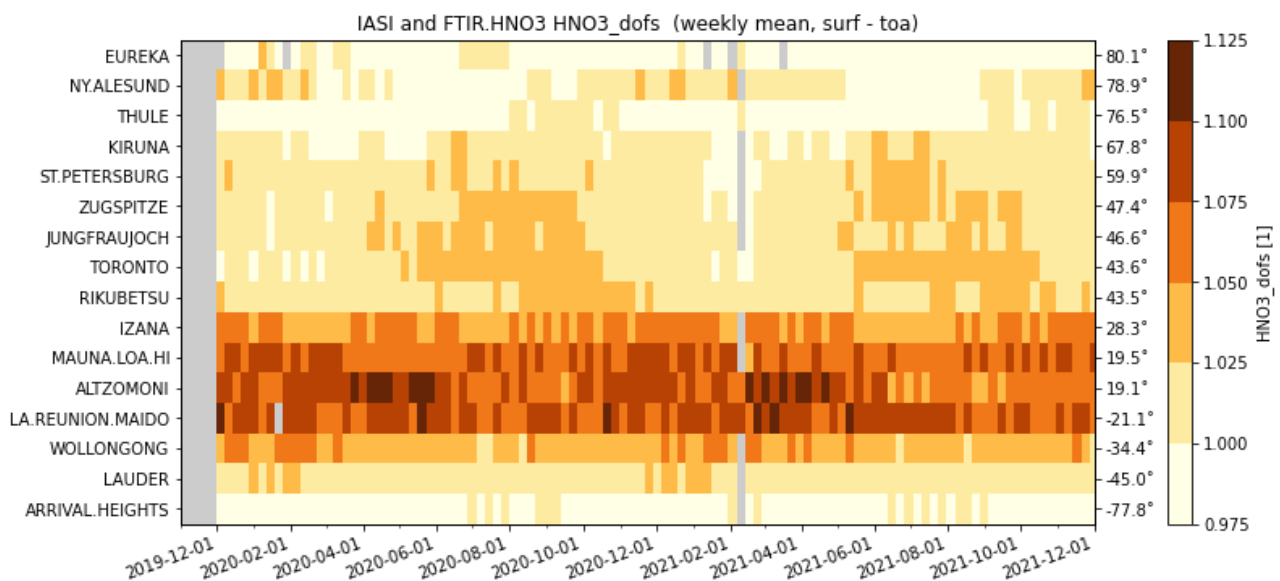


Figure 2.4 Mosaic of IASI-B HNO₃ degrees of freedom (DOF) at the different NDACC sites for the period 2020-2021. Similar to Figure 2.1, sites are sorted according to latitude. At the tropical sites a lightly higher DOF is observed which is reducing to values slightly below 1 at the high latitude sites.

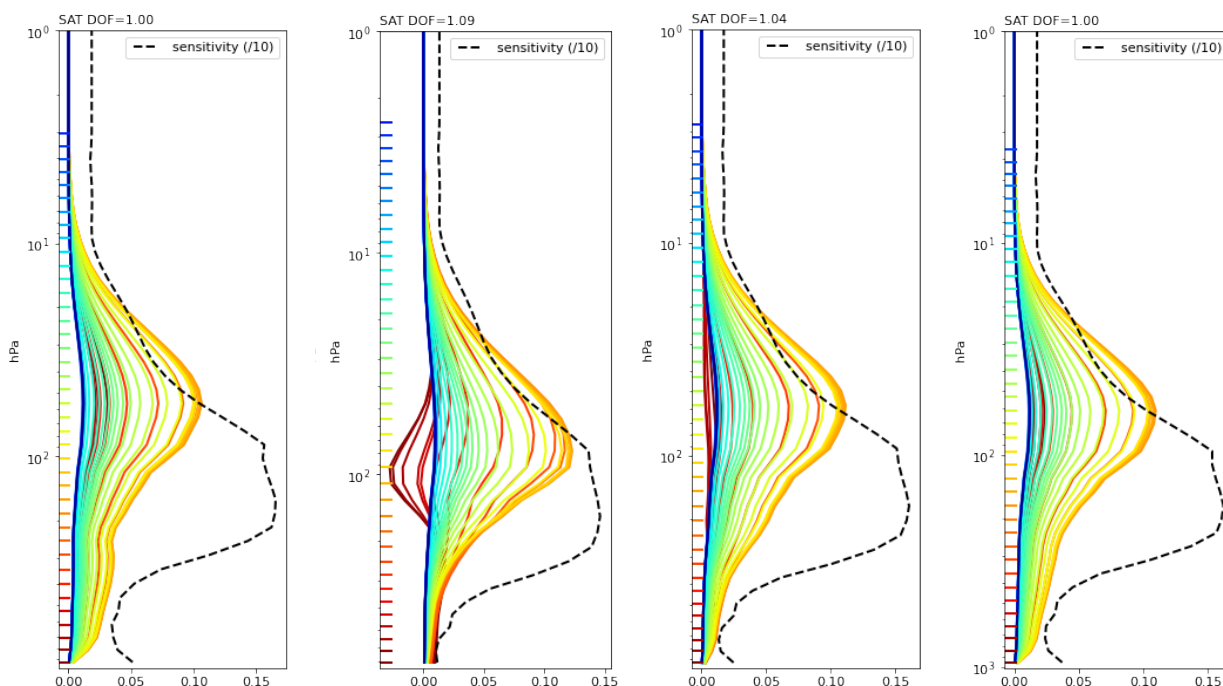


Figure 2.5 Typical averaging kernels for 4 IASI B pixels at (from left to right) Arrival Heights (Antarctic station), Alzomoni (Mexico), Jungfraujoch (Switzerland) and Thule (Greenland). The sensitivity curve (sum of AVK rows) near the surface shows an increase towards 0.05 near the surface for the high latitude sites. The averaging kernels shown here act on VMR profiles relative to the *a-priori*.

2.2. Comparison methodology

Each FTIR measurement is co-located to all IASI pixels within a time difference of 6 hours and within a distance of 200 km around the effective location of the FTIR measurement. This effective location is derived from an effective altitude, which is in turn obtained as a weighted mean of the altitude using the HNO₃ partial column profile as weight. The effective altitude is then projected along the line of sight of the FTIR measurement and can reach distances up to more than 300km for the high solar zenith measurements. Taking into account the effective location has a positive effect on the overall comparison statistics and reduces the bias by 1% for the high latitude stations.

For each co-located pair consisting of a single FTIR and IASI measurement, a sequence of operations is performed aiming to reduce the influence of the two *a priori* profiles used in the FTIR and IASI retrieval methods (Rodgers *et al.*, 2003). A first step consists of regridding the FTIR *a priori* and retrieved profiles to the IASI grid. Secondly, the regridded FTIR *a priori* is substituted in the IASI retrieval and the third and final step consists of using the smoothing equation by applying the IASI averaging kernel on the FTIR retrieved and regridded profile and using the FTIR *a priori* as a common prior. All these steps follow the methodology described in Rodgers *et al.*, 2003.

Regridding is done such that the total mass HNO₃ is conserved (Langerock *et al.*, 2014) and possible vertical mismatches between the station surface and the satellite pixel surface are corrected by extending the regridded FTIR profiles by the extrapolated FTIR *a priori*. All profiles in the comparison are plotted for a single measurement pair in Figure 2.6.

JUNGFRAUJOCH FTIR.HNO3_ULG002 measurement (04/12/2019-08:02:02) against SAT (09:36:09)
 co-location: 45.88N(GB)|45.88N(SAT) 8.93E(GB)|10.56E(SAT)

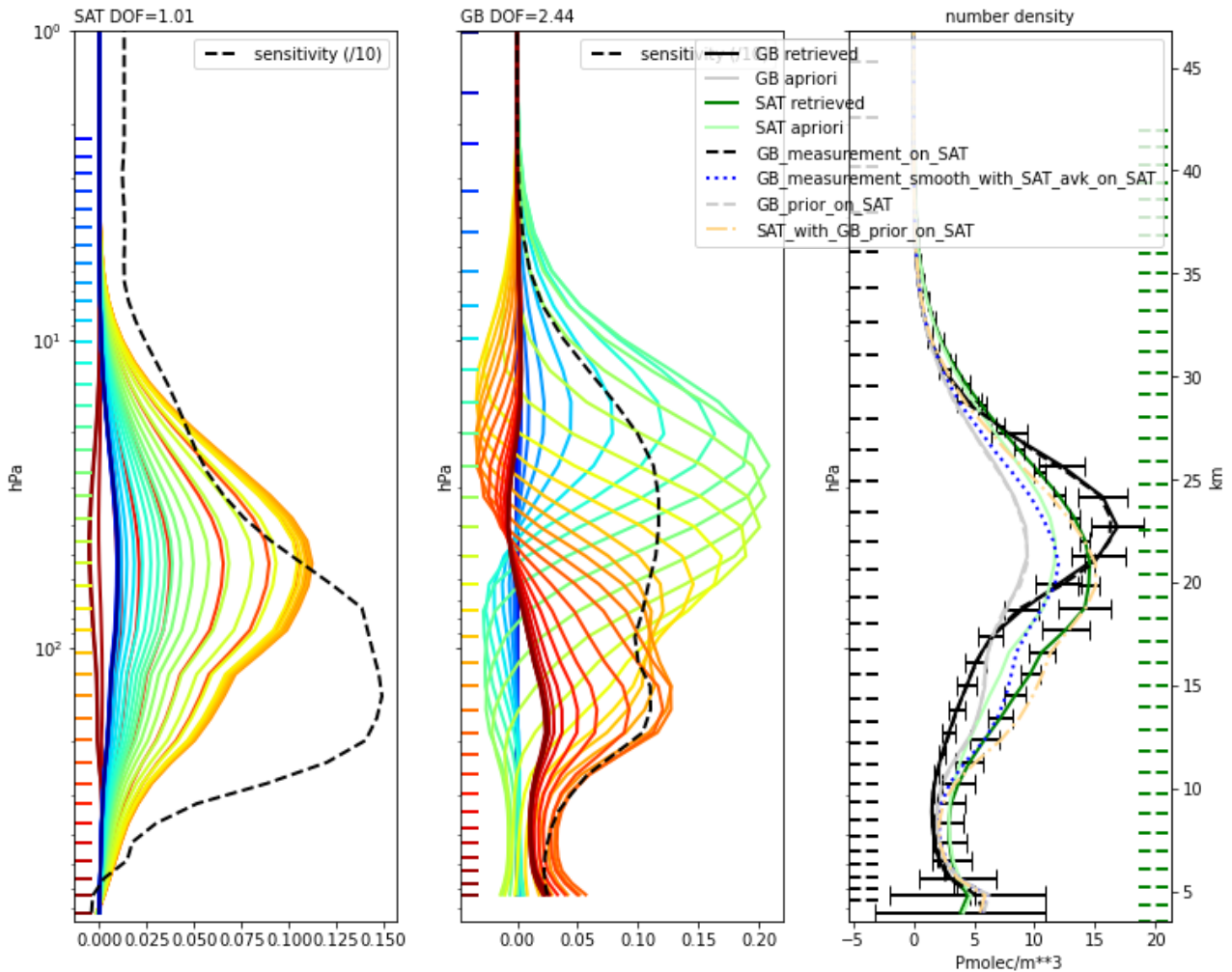


Figure 2.6 Detailed comparison plot for of a single IASI-B HNO₃ pixel (green profile in the right panel) against a co-located FTIR measurement (black profile). The right panel contains all profiles calculated for this comparison, the most left plot is the IASI AVK, the middle panel shows the FTIR AVK (all AVK act on VMR profiles relative to the *a priori*).

As mentioned in Section 2.1, the common prior is chosen to be the FTIR *a priori* profile since the IASI *a priori* profile shows an increased bias for the tropical stations and this leads to a non-negligible systematic smoothing error in the comparison statistics. Here the comparison methodology deviates from the methodology described in Ronsmans *et al.*, 2016, where the IASI *a priori* is chosen as a common prior.

From the IASI averaging kernels shown in Figure 2.5, the IASI retrievals at higher latitudes with reduced DOF have an artefact where the AVK rows corresponding to the lower altitudes (<5km) have increased sensitivity. This causes a compensation in the FTIR *a priori* substitution in the IASI profiles and a change in the smoothed FTIR profile below at altitudes <5km, see for instance the mosaic plot of profile differences for Thule in Figure 2.7.

Similar to Ronsmans *et al.*, 2016 we therefore calculate partial columns between 5km and 35km from the profile. Above 35km there is no sensitivity and below 5km the comparison may suffer from an artefact in the IASI kernels. This has only a small effect on the column statistics due to the low concentrations at these altitudes.

As a final step, all co-located pairs that originate from a single FTIR measurement are averaged. This averaging is done on the partial columns between the given boundaries. Only FTIR measurements with at least four co-located IASI profiles are taken into account and from all co-located IASI profiles only the 10 closest pixels are averaged. A similar averaging methodology was also used in Ronsmans *et al.*, 2016 and reduces the noise on the IASI measurements (see also the conclusions).

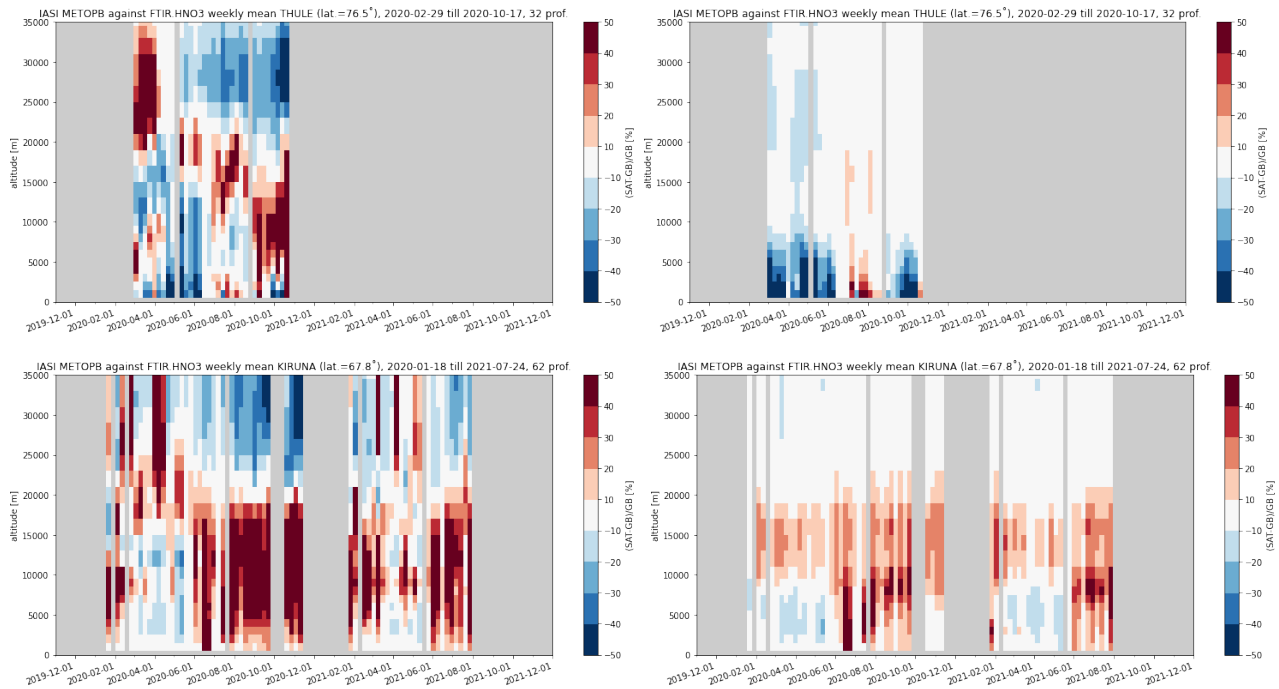


Figure 2.7 Mosaic plot of vertical profile differences at the high latitude station Thule (top row) and Kiruna (bottom row) for IASI-B to demonstrate the effect of the smoothing operation. The left plot shows the difference of the regridded FTIR profile and the IASI profile (containing the FTIR *a priori*) The right panel shows the difference of the smoothed FTIR profile and the IASI profile (containing the FTIR *a priori*).

2.3. Comparison statistics.

Differences are calculated using either the smoothed FTIR columns against the IASI columns (containing the FTIR *a priori*) or directly using the FTIR NDACC data without any modification. Table 2.1 and Table 2.2 provide the details per station for the relative differences and Pearson correlation coefficients for both the direct comparison and the comparison using the smoothed FTIR columns.

To interpret the statistics, the following remarks on the FTIR data are relevant:

1. Eureka, Ny Ålesund, Zugspitze, St Petersburg and La Reunion provide only a few measurements in 2020, and are statistically less relevant
2. The typical FTIR uncertainty is estimated at 8% and increases to 12% at the high latitude stations. The random uncertainty contribution is typically around 3% while the systematic uncertainty (main contributor is the uncertainty on spectroscopic parameters) is typically 10%
3. The statistics in Table 2.1 and Table 2.2 are restricted to the time period to Dec 2019 Dec 2020 because only a few sites provide recent measurements in 2021

IASI NRT data has the following characteristics ([AD2, PUM]):

1. Statistics for IASI-A and C are very similar to IASI-B and are therefore left out from the figures.
2. The IASI prior is too high in the tropics and the FTIR prior is therefore used as the common prior.

3. The typical reported IASI uncertainty is estimated at 10% and increases to 20-25% at the tropical sites Mauna Loa, Altzomoni, Reunion. The combined uncertainty on the relative differences (satellite minus groundbased) is ranging from 15% to 25%.
4. From the PRD, the required target product accuracy is 35% with an optimal value of 10%.

Comparison statistics up to January 1 2021 are presented in Table 2.1 (direct comparison) and Table 2.2 (smoothing enabled) and correspond to the mosaic visualisation in Figure 2.8.

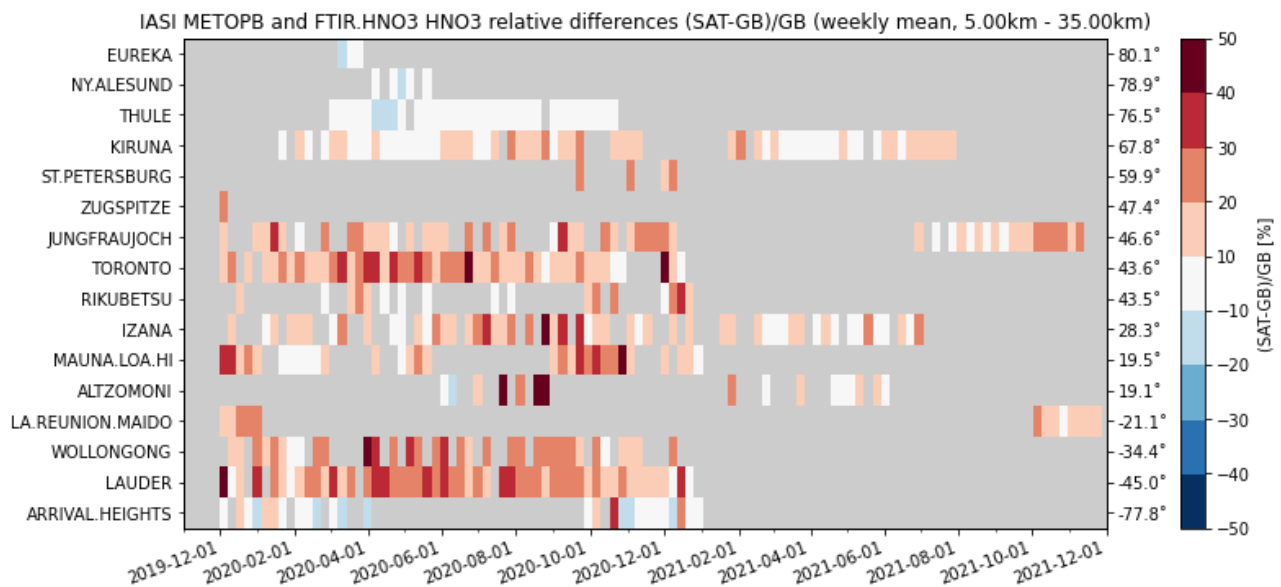


Figure 2.8 Mosaic of weekly mean relative differences for the FTIR smoothed and the IASI columns (containing the FTIR *a priori*). For most sites a positive bias of around 20% is observed except at the high latitude sites (Eurka, Ny Alesund and Arrival Heights) having a reduced bias.

Table 2.1. Statistics for the direct comparison between IASI Metop-B/C and FTIR HNO₃ total columns for 2020 (the column “std” is the standard deviation of the local FTIR columns relative to the standard deviation of the IASI columns, R is the Pearson correlation coefficient, rel. diff. is the mean of the relative differences IASI minus FTIR in percentage).

	Metop-B					Metop-C				
	# meas.	std.	R	rel. diff.	std. rel. diff.	# meas.	std.	R	rel. diff.	std. rel. diff.
EUREKA	112	1.2	0.89	11.66	14.98	103	1.2	0.92	8.05	12.83
NY.ALESUND	14	1.3	0.89	-10.08	5.57	14	1.2	0.56	-11.95	10.87
THULE	622	1.1	0.86	-2.93	8.71	617	1.2	0.8	-3.8	9.3
KIRUNA	417	1	0.95	11.7	8.96	410	1	0.95	10.73	8.05
ST.PETERSBURG	14	1.1	0.88	26.32	8.09	10	1	0.78	23.25	10.65
ZUGSPITZE	24	0.9	0.91	24.16	6	17	1.3	0.94	22.52	5.58
JUNGFRAUJOCH	457	0.9	0.91	21.68	8.34	440	0.9	0.93	20.55	7.47
TORONTO	491	0.7	0.89	23.46	12.2	490	0.7	0.87	22.04	13.08
RIKUBETSU	18	0.8	0.9	14.18	9.53	18	0.7	0.95	9.89	9.2
IZANA	196	1	0.85	17.81	11.58	198	1	0.84	17.19	11.42
MAUNA.LOA.HI	420	1.1	0.89	20.42	12.47	385	1	0.9	19.66	12.02
ALTZOMONI	30	0.4	0.57	40.32	21.04	42	0.6	0.81	30.41	10.94
LA.REUNION.MAIDO	31	0.8	0.67	17.27	8.23	28	1.4	0.72	14.42	6.31
WOLLONGONG	597	0.8	0.92	23.3	9.69	609	0.8	0.9	21.02	9.63
LAUDER	809	0.8	0.85	23.57	11.4	761	0.8	0.86	21.48	10.52
ARRIVAL.HEIGHTS	222	1.1	0.93	0.51	15.13	213	1.1	0.92	0.13	16.45
Mean		0.94	0.86	16.46	10.75		1	0.85	14.1	10.27

Table 2.2. Statistics overview for the comparison with smoothing between IASI Metop-B/C and FTIR HNO₃ total columns for 2020 (table columns have similar meaning as in Table 2.1).

	# meas.	std.	R	rel. diff.	std. rel. diff.	# meas.	std.	R	rel. diff.	std. rel. diff.
EUREKA	112	1.1	0.9	2.38	11.35	103	1.1	0.91	-1.3	10.28
NY.ALESUND	14	1.2	0.8	-11.1	6.71	14	1	0.46	-13.02	11.39
THULE	622	1	0.86	-2.89	9.09	617	1.1	0.81	-3.75	9.45
KIRUNA	417	1	0.95	11.13	8.66	410	1	0.95	10.21	7.93
ST.PETERSBURG	14	1.1	0.93	21.59	6.8	10	1.1	0.82	20.38	10.82
ZUGSPITZE	24	0.8	0.92	22	5.54	17	1.2	0.92	21.47	4.7
JUNGFRAUJOCH	457	0.9	0.91	20.22	8.85	440	0.9	0.92	19.09	7.94
TORONTO	491	0.8	0.88	20.29	12.08	490	0.8	0.86	19.05	13.14
RIKUBETSU	18	0.8	0.9	14.21	9.84	18	0.7	0.95	9.88	9.26
IZANA	196	0.9	0.85	17.17	11.72	198	1	0.83	16.65	11.45
MAUNA.LOA.HI	420	1.1	0.9	18.36	11.82	385	1	0.91	17.41	11.4
ALTZOMONI	30	0.3	0.43	31.7	24.57	42	0.6	0.73	22.25	12.01
LA.REUNION.MAIDO	31	0.7	0.68	19.19	8	28	1.3	0.71	16.04	6.12
WOLLONGONG	597	0.8	0.92	22.18	9.67	609	0.8	0.91	19.9	9.63
LAUDER	809	0.8	0.86	22.45	11	761	0.8	0.88	20.37	10.21
ARRIVAL.HEIGHTS	222	1	0.94	-1.58	14.21	213	1	0.93	-2.75	14.04
Mean		0.9	0.85	14.21	10.62		0.96	0.84	11.99	9.99

3. DISCUSSION AND CONCLUSIONS

From Table 2.2. all individual stations have a bias estimate below the product required target accuracy of 35% [AD2] for both the IASI B (O3M-81) and IASI-C (O3M-336) target products.

From the statistics tables 2.1 and 2.2 we learn that the comparison of the smoothed columns reduces the mean relative difference (bias) with approximately 2%: for IASI-B from 16.46% (direct comparison) to 14.2% (smoothing enabled) and for IASI-C from 14.1% to 12%. These bias estimates are comparable to the reported combined measurement uncertainties. On a network basis the 10% optimal accuracy set in the product requirement document [AD2] is nearly met for both O3M-81 and O3M-336 products when taking the FTIR data as a reference. At high latitude stations the bias is significantly reduced to values close to zero or slightly below zero: -2% at Arrival Heights and -3% at Thule for IASI-B, see Figure 3.1. These statistics confirm the conclusions in Ronsmans *et al.*, 2016, where a similar positive overall bias of approximately 10% for IASI was determined.

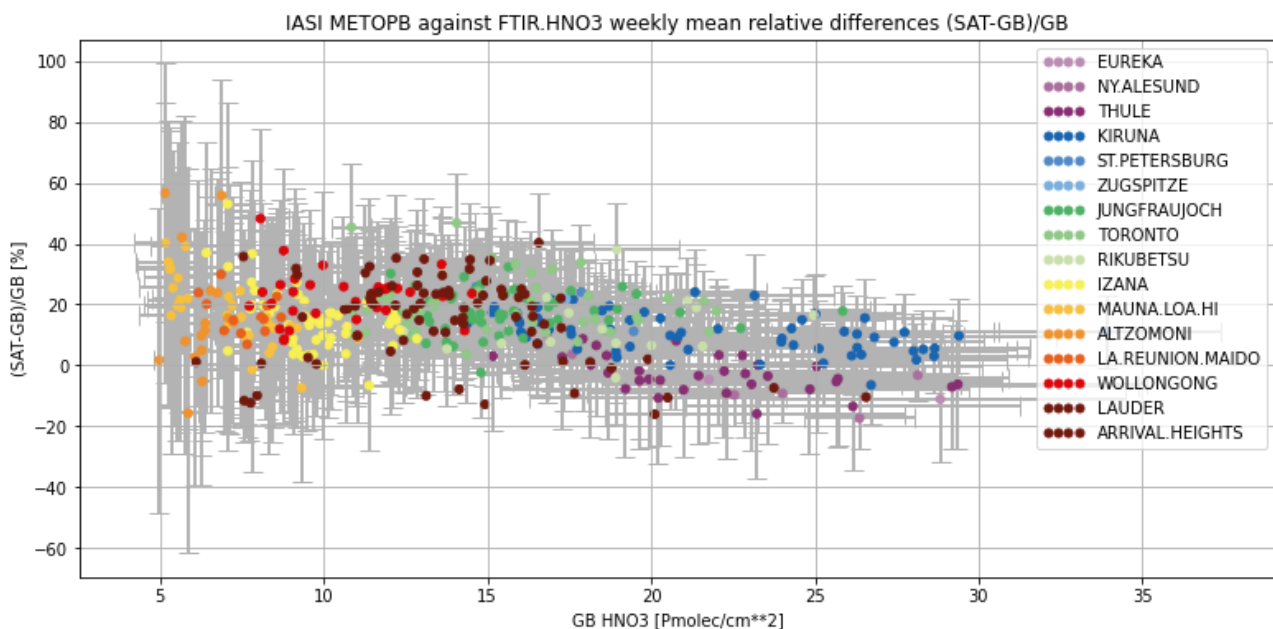


Figure 3.1 Weekly mean bias vs the measured FTIR total column. Low concentrations at the tropical sites show a systematic positive bias. While the bias nearly vanishes for the higher concentration seen during the local winter at the high latitude sites.

The overall correlation is 0.85. The smoothing operation has a minor effect on the overall correlation. The ratio of the standard deviations of the two HNO₃ column time series FTIR and IASI is very close to the ideal value of 1 and indicate that both the IASI and FTIR data products detect the same signal and variability in HNO₃ (see Figure 3.2)

Although the comparison is limited to one year which prevents us from discussing seasonal cycles and trends, from Figure 2.8 we can confirm the same conclusion as in Ronsmans *et al.*, 2016 that no clear seasonal dependence in the bias is observed.

The standard deviation of the relative differences is on average 10% and reflects the remaining noise on the IASI and FTIR columns (the random uncertainty for the FTIR is estimated 3%). A comparison setup where each FTIR is co-located to the closest IASI pixel has an augmented standard deviation on the relative differences of around 20% and a related decrease in the correlation R=0.6. The choice to average up to 10 IASI pixels is therefore justified since it reduces the IASI random uncertainty significantly and has a significant impact on the estimated correlation.

Because the statistics are based on only one year of data, all estimates should still be considered preliminary and should be confirmed when a longer time series is available.

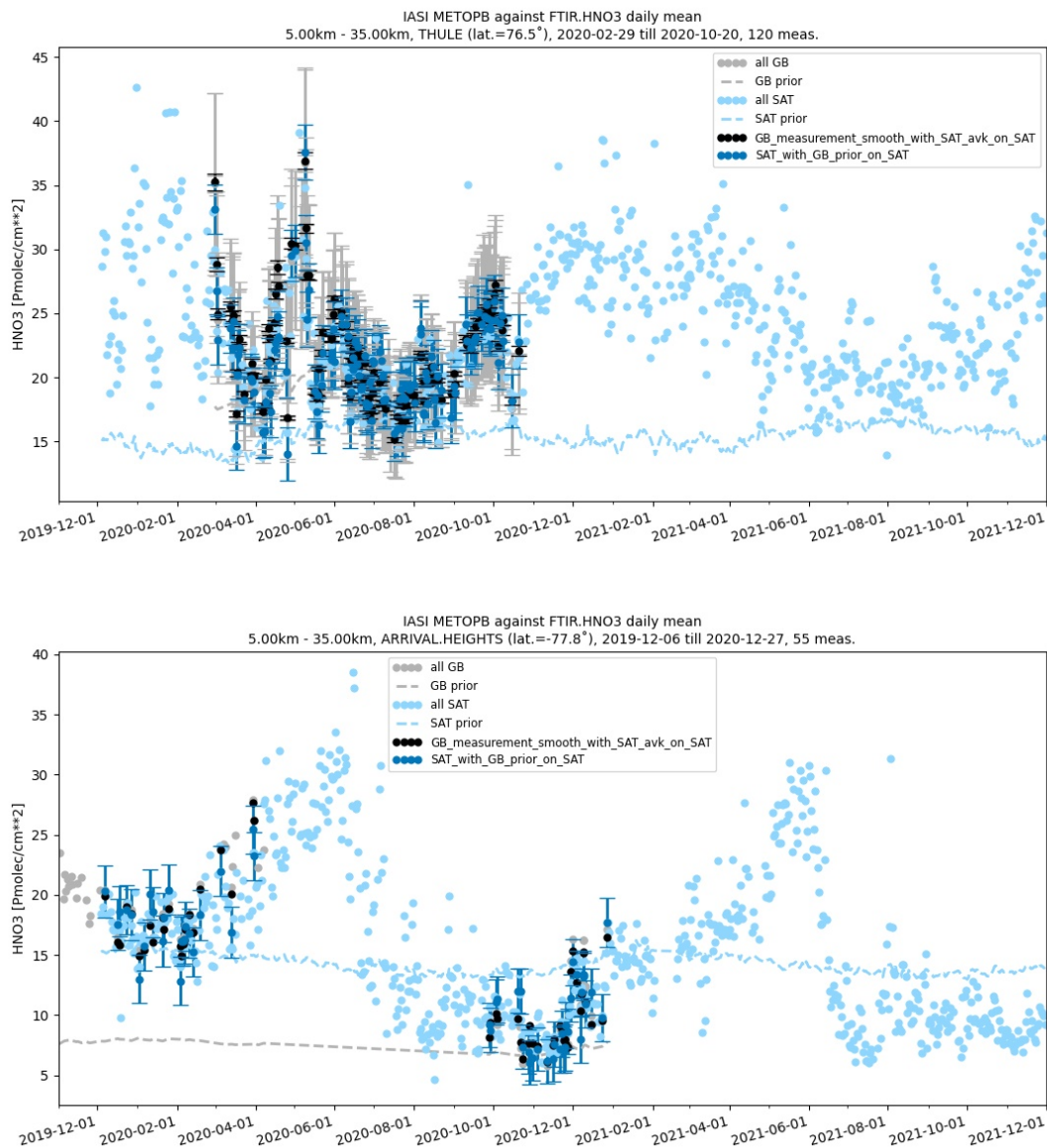


Figure 3.2 Time series showing the seasonal changes in HNO₃ at the high latitude site at Thule (top) and Arrival Heights (bottom). The IASI and FTIR columns detect the same HNO₃ signal.

Acknowledgments: The data used in this publication were obtained as part of the Network for the Detection of Atmospheric Composition Change ([NDACC](#)) and are publicly available.

4. REFERENCES

4.1. Applicable documents

[AD1] FORLI-HNO3 Product Specification, Requirement And Assessment SAF/O3M/ULB/FORLICO_PSRA Issue 1, 21/01/2015

[AD2] Product Requirements Document SAF/AC/FMI/RQ/PRD/001 Issue 1.9.1, 03/02/2022

[PUM] Product User Manuel, SAF/AC/ULB/PUM/004, Issue 1.1, 27/04/2021.

4.2. Reference documents

Hilton, F.; August, T.; Barnett, C.; Bouchard, A.; Camy-Peyret, C.; Clarisse, L.; Clerbaux, C.; Coheur, P.-F.; Collard, A.; Crevoisier, C.; Dufour, G.; Edwards, D.; Fajjan, F.; Fourrié, N.; Gambacorta, A.; Gauguin, S.; Guidard, V.; Hurtmans, D.; Illingworth, S.; Jacquinet-Husson, N.; Kerzenmacher, T.; Klaes, D.; Lavanant, L.; Masiello, G.; Matricardi, M.; McNally, T.; Newman, S.; Pavelin, E.; Péquignot, E.; Phulpin, T.; Remedios, J.; Schlüssel, P.; Serio, C.; Strow, L.; Taylor, J.; Tobin, D.; Uspensky, A. & Zhou, D. Hyperspectral Earth Observation with IASI. *Bull. Am. Meteorol. Soc.*, 93(3), 347-370, doi: 10.1175/BAMS-D-11-00027.1, 2012.

Clerbaux, C.; Boynard, A.; Clarisse, L.; George, M.; Hadji-Lazaro, J.; Herbin, H.; Hurtmans, D.; Pommier, M.; Razavi, A.; Turquety, S.; Wespes, C. & Coheur, P. F. Monitoring of atmospheric composition using the thermal infrared IASI/MetOp sounder. *Atmos. Chem. Phys.*, 9(16):6041-6054, 2009

Hurtmans, D.; Coheur, P.; Wespes, C.; Clarisse, L.; Scharf, O.; Clerbaux, C.; Hadji-Lazaro, J.; George, M. & Turquety, S. FORLI radiative transfer and retrieval code for IASI. *J. Quant. Spectrosc. Radiat. Transfer*, 113, 1391-1408, 2012.

Langerock, B., De Mazière, M., Hendrick, F., Vigouroux, C., Desmet, F., Dils, B., and Niemeijer, S.: Description of algorithms for co-locating and comparing gridded model data with remote-sensing observations, *Geosci. Model Dev.*, 8, 911–921, <https://doi.org/10.5194/gmd-8-911-2015>, 2015

Rinsland, C. P., Zander, R., and Demoulin, P.: Ground-based in- frared measurements of HNO3 total column abundances: Long- term trend and variability, *J. Geophys. Res.*, 96, 9379–9389, doi:10.1029/91JD00609, 1991

Rodgers, C. D. *Inverse methods for atmospheric sounding: Theory and Practice*, Series on Atmospheric, Oceanic and Planetary Physics - Vol. 2. World Scientific, Singapore, New Jersey, London, Hong Kong, 2000

Rodgers, C. D. and Connor, B. J.: Intercomparison of re- mote sounding instruments, *J. Geophys. Res.*, 108, 4116, doi:10.1029/2002JD002299, 2003.

Ronsmans, G., Langerock, B., Wespes, C., Hannigan, J. W., Hase, F., Kerzenmacher, T., Mahieu, E., Schneider, M., Smale, D., Hurtmans, D., De Mazière, M., Clerbaux, C., and Coheur, P.-F.: First characterization and validation of FORLI-HNO3 vertical profiles retrieved from IASI/Metop, *Atmos. Meas. Tech.*, 9, 4783–4801, <https://doi.org/10.5194/amt-9-4783-2016>, 2016

Vigouroux, C., De Mazière, M., Errera, Q., Chabrilat, S., Mahieu, E., Duchatelet, P., Wood, S., Smale, D., Mikuteit, S., Blumen- stock, T., Hase, F., and Jones, N.: Comparisons between ground- based FTIR and MIPAS N2O and HNO3 profiles before and af- ter assimilation in BASCOE, *Atmos. Chem. Phys.*, 7, 377–396, doi:10.5194/acp-7-377-2007, 2007

Vigouroux, C., Langerock, B., Bauer Aquino, C. A., Blumenstock, T., Cheng, Z., De Mazière, M., De Smedt, I., Grutter, M., Hannigan, J. W., Jones, N., Kivi, R., Loyola, D., Lutsch, E., Mahieu, E., Makarova, M., Metzger, J.-M., Morino, I., Murata, I., Nagahama, T., Notholt, J., Ortega, I., Palm, M., Pinardi, G., Röhling, A., Smale, D., Stremme, W., Strong, K., Sussmann, R., Té, Y., van Roozendaal, M., Wang, P., and Winkler, H.: TROPOMI–Sentinel-5 Precursor formaldehyde validation using an extensive network of ground-based Fourier-transform infrared stations, *Atmos. Meas. Tech.*, 13, 3751–3767, <https://doi.org/10.5194/amt-13-3751-2020>, 2020

Wespes, C., Hurtmans, D., Clerbaux, C., Santee, M. L., Martin, R. V., and Coheur, P. F.: Global distributions of nitric acid from IASI/MetOP measurements, *Atmos. Chem. Phys.*, 9, 7949–7962, doi:10.5194/acp-9-7949-2009, 2009